Crystal field effect on a bilayer Bethe lattice

Osman Canko and Erhan Albayrak
Department of Physics, Erciyes University, 38039, Kayseri, Turkey
(Received 2 June 2006; revised manuscript received 28 September 2006; published 19 January 2007)

The influence of the crystal field on the phase diagrams of the bilayer spin-1 Ising model on the Bethe lattice is studied in terms of the intralayer coupling constants J_1 and J_2 of the two layers and interlayer coupling constant J_3 between the layers for given values of the coordination number q by using the recursion relation scheme. The six distinct ground-state configurations of the model are obtained on the $(J_2/J_1, J_3/qJ_1)$ plane with $J_1>0$, the ferromagnetic coupling, for given values of the crystal field. Then, the phase diagram of the system is obtained on the $(kT/J_1, J_3/J_1)$ plane for given values of the crystal field and $\alpha=J_2/J_1$ with $q=4$ corresponding to the square lattice in real lattice systems. It was found that the system presents both first- and second-order phase transitions, therefore, tricritical points. The paramagnetic phase was also divided into two phases, P_+ and P_-, by studying the thermal behavior of the quadrupolar moments of the two layers.

DOI: 10.1103/PhysRevE.75.011116 PACS number(s): 05.50.+q, 68.35.Rh, 64.60.Cn

I. INTRODUCTION

The magnetic properties of the multilayer structures or thin films are important and attempts to understand them have led to a deep insight into their fundamental structures. The magnetic properties are obviously different from those of the corresponding bulk and semi-infinite systems. Owing to the development of the science and technology, the magnetic thin films consisting of various magnetic layered structures or superlattices have been manufactured, therefore, they have been receiving intense attention in recent years for both theoretical and experimental reasons. These materials are made up with multiple layers of different magnetic substances, hence there is a high potential for technological advances in information storage and retrieval and in synthesis of new magnets for a variety of applications [1], besides they also exhibit some interesting magnetic properties such as giant magnetoresistance [2], surface magnetic anisotropy [3], enhanced surface magnetic moment [4], and surface magnetoelastic coupling [5].

Maybe the simplest and the cornerstone of almost every study in magnetic systems are usually carried out with spin 1/2, as a result the multilayered structures or Ising films containing spin 1/2 are studied theoretically with many techniques and for many physical reasons such as in understanding the critical behaviors of such layered systems. Therefore, these systems were investigated within several different frameworks, that is in the mean-field theory (MF) [6], within the framework of the effective field theory (EFT) [7], and by the use of Monte Carlo simulations (MC) [8].

Besides the methods mentioned above, we could also report some studies made with other techniques for spin 1/2, that is, the ground state of the square lattice bilayer quantum antiferromagnet with nearest and next-nearest neighbor interlayer interaction by means of the modified spin-wave method [9], the symmetric two-layer Ising model by the corner transfer matrix renormalization group method to calculate the critical points and critical exponents [10], a two-layer Ising system, in which the coupling strengths within each layer are in general unequal and also differ from the coupling strength between the layers, by means of a mean-field theory, a generalized mean-field theory, a scaling approach and high-temperature series expansions [11], a simple criterion which allows for the straightforward determination of the order-disorder critical temperatures is found and which predicts that $\beta=0.2656$ for the two coupled layers of Ising spins [12], a simple model for the temperature and the thickness dependence of the direction of magnetization of ferromagnetic thin films or sandwiches [13], the magnetic properties of two different magnetic films separated by a nonmagnetic spacer by means of the variational cumulant expansion [14], the multilayer square lattice Heisenberg antiferromagnet with up to six layers in terms of series expansions [15], the infinite ferromagnetic AB_1AB_2 superlattice and $A(n_a)B(n_b)$ sandwich structures in a linear cluster approximation (LCA) [16] and a simple cubic-type structure to determine the magnetic properties for superlattices of periodic $A_k(A_pB_{1-p})_1B_h$ formula consisting of k layers of spin-1/2 A ions, h layers of spin-1/2 B ions, and a single layer disordered alloy interfaces between them [17].

We should also bring up that the spin-1/2 Ising model for the multilayered structures are also studied on the fictitious trees and lattices, i.e., a variety of the aspects of a bilayer system of Ising spins including accurate estimates of the critical temperature for ferromagnetic interactions, scaling of the critical temperature when the interlayer interaction goes to zero, and approximations of the phase diagrams for the case when antiferromagnetic interlayer interactions are present including location of the tricritical point [18] on Husimi trees, the behavior of the Ising thin films through the use of layered Bethe lattices and Husimi trees [19], the role of the interlayer coupling between CuO_2 planes on bilayer-group high-T_c superconductors within a simple randomly decorated bilayer Ising model and a Bethe-lattice approach [20], and the exact expressions for the free energy and the magnetization of an Ising model on a two-layer Bethe lattice by using an iteration technique in a pairwise approach [21].

The spin-1/2 Ising model does not include the crystal field, hence in order to study the crystal field effects on the multilayered structures or thin films one has to use at least spin-1 Ising models. As a result, the spin-1 Ising system has attracted a great deal of attention and was introduced for studying the superfluidity and phase separation in Helium mixtures [22], afterwards this model was extended for the systems characterized with three states such as solid-liquid-gas systems, multicomponent fluid and liquid crystal mixtures [23], microemulsions [24], semiconductor alloys [25], ternary mixtures [26], electron conduction models [27], martensitic transformations [28], and two-dimensional Blume-Emery-Griffiths-Potts model [29].

Therefore, the multilayered systems consisting of spin 1 are also of interest: the effects of surface single-ion anisotropy and surface dilution on surface phase transitions of a semi-infinite Ising model with diluted spins on the surface were investigated by the use of an effective field theory [30], ellipsometric and calorimetric studies of argon and krypton adsorbed on triangular lattice graphite substrates have found a sequence of apparent reentrant layering transitions between integer-plus-one-half coverages [31], which motivated the study of preroughening and layering transitions on triangular lattice substrates by the use of the solid-solid models [32]. The magnetic phase diagram of a thin film is determined at $T=0$ by including the exchange coupling, the magnetic dipole coupling, as well as second- and fourth-order lattice anisotropies [33]. The complete global phase diagram for a spin-1 bilayer Blume-Emery-Griffths (BEG) model is studied by the use of cluster variational theory in the pair approximation [34], motivated by the experiments of the effect of the interlayer exchange interaction on the magnetic properties of coupled Co/Cu/Ni trilayer that was studied theoretically and the magnetization and susceptibility of the coupled ferromagnetic trilayers calculated with a Green's function-type theory [35], respectively. The order-disorder layering transitions are studied in the presence of a variable crystal field by using the Monte Carlo simulations and mean-field theory [36], respectively. The effect of the transverse field on bulk melting and layering sublimation transitions of the BEG model was studied by using the mean-field theory [37]. The phase transitions of a transverse spin-1 Ising L-layer film of simple cubic symmetry with nearest-neighbor exchange interactions was examined within the framework of the effective-field theory and again using the effective-field theory with a probability distribution technique that accounts for the self-spin-correlation functions, the layer longitudinal magnetizations and quadrupolar moments of a spin-1 Ising film and their averages are examined [38], respectively.

We should also note that the exact solutions for the realistic systems on regular lattices are generally unavailable, therefore, one usually relies on approximation methods to obtain, at least, a qualitative picture for the phase diagrams of the considered system at hand. As a result, one may even introduce a lattice-like fictitious tree to find exact or approximate solutions of the model. A Bethe lattice is such a lattice, which is an infinitely Cayley or regular tree that is a connected graph without circuits and historically gets its name from the fact that its partition function is exactly that of an Ising model on the Bethe approximation [39]. The importance is that the Bethe lattice is an infinite tree gives us the negligible boundary effects, therefore, far from the boundary sites that is deep inside the Cayley tree, now Bethe lattice, all the sites become equivalent, thus studying the behavior of one spin, named as the central spin, is enough to obtain the full picture of the system. We should also comment that the Bethe lattice calculations provides exact solutions and results of which qualitatively better approximations for the regular lattices than solutions obtained by the conventional mean-field theories [40]. In addition, the cluster variation method in the pair approximation studies on regular lattices yield results that are exact for the same model on the Bethe lattice [41]. Of course, the Bethe lattice considerations also have some limitations, that is it predicts a transition temperature higher than that for a regular lattice and it is not reliable for predicting critical exponents [21], where also the correspondence of the Bethe lattice with regular lattices and real physical systems and whether it can be embedded into a finite-dimensional Euclidean space are also discussed. Therefore, in this work we study the bilayer spin-1 Ising system on the Bethe lattice by using the recursion relations obtained by the pairwise approach [21].

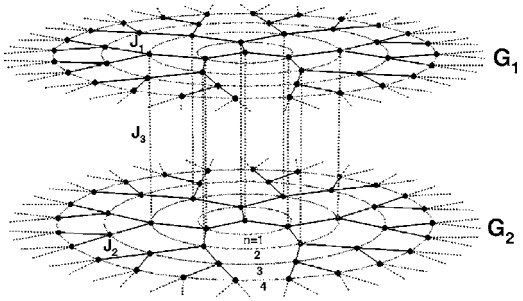

FIG. 1. The two-layer Bethe lattice of coordination number $q=3$. G_1 and G_2 refer to the upper and lower layers containing the spins labeled as S_i and $\sigma_{i'}$, respectively. While J_1 and J_2 are the bilinear interactions of spins in G_1 and G_2, J_3 is the one for the adjacent spins of G_1 and G_2.

The rest of the paper is organized as follows. In Sec. II, the bilayer Ising model is introduced and then the ground-state phase diagrams are obtained and discussed. Sec. III is devoted to obtaining the order-parameters and the free energy of the system in terms of the recursion relations exactly. In Sec. IV we have presented the phase diagrams of the model for given values of the crystal field D/qJ_1 and $\alpha=J_2/J_1$ on the $(kT/J_1, J_3/J_1)$ plane for $q=4$. Finally, in the last section we give a brief summary and concluding remarks.

II. BILAYER BETHE LATTICE AND ITS GROUND STATES

The bilayer Bethe lattice is an extension of its one-layer version [42]. The one-layer version consists of a central spin which may be called the first generation spin. This central spin has q nearest neighbors (NN), i.e., coordination

number, which forms the second-generation spins. Each spin in the second-generation is joined to $(q-1)$ NN's. Therefore, in total this generation has $q(q-1)$ NN's which form the third generation and so on to infinity. We consider two identical layers of Bethe lattices G_1 and G_2 which are placed parallel to each other forming the bilayer Bethe lattice as shown in Fig. 1. In each layer, every spin interacts with its NN and the corresponding adjacent spins in the other layer whose sites are labeled by i and i', respectively as seen in Fig. 1.

The Ising Hamiltonian of such a bilayer Bethe lattice system is given as

$$\mathcal{H} = -J_1 \sum_{\langle ij \rangle} S_i S_j - J_2 \sum_{\langle i'j' \rangle} \sigma_{i'} \sigma_{j'} - J_3 \sum_{\langle ii' \rangle} S_i \sigma_{i'} - D \sum_i S_i^2 - D \sum_{i'} \sigma_{i'}^2, \tag{1}$$

where S_i and $\sigma_{i'}$ take the values ± 1 and 0, and refer to the spins of G_1 and G_2, J_1 and J_2 are the intralayer bilinear interactions and, the first and second summation is over all sites of G_1 and G_2, respectively. J_3 is the interlayer bilinear interaction of NN spins between the layers, therefore the third summation runs over all the adjacent neighboring sites of G_1 and G_2. The layers are assumed to be under the influence of equal crystal field D, so the fourth and final sums run over all the lattice sites in each layer, respectively.

In order to define the system completely one should consider five order parameters to obtain the critical behaviors of the model. Two of these order parameters correspond to thermal average of total spins of layers G_1 and G_2, that is the magnetizations of layers, defined as follows:

$$m_1 = \frac{1}{N} \sum_{i=1}^{N} \langle S_i \rangle, \quad m_2 = \frac{1}{N} \sum_{i'=1}^{N} \langle \sigma_{i'} \rangle. \tag{2}$$

But, instead of these order parameters, it is much appropriate to use the total magnetization m and the staggered magnetization η which are defined as

$$m = \frac{1}{2}(m_1 + m_2), \quad \eta = \frac{1}{2}(m_1 - m_2). \tag{3}$$

The third order parameter corresponds to the interlayer interaction of adjacent NN spins of the layers, called as the spin-spin correlation function between the two layers, is defined as

$$\rho = \frac{1}{N} \sum_{i=i'=1}^{N} (\langle S_i \sigma_{i'} \rangle - \langle S_i \rangle \langle \sigma_{i'} \rangle). \tag{4}$$

The last two order-parameters of the model are the quadrupolar order parameters of the layers defined as

$$Q_1 = \frac{1}{N} \sum_{i=1}^{N} \langle S_i^2 \rangle, \quad Q_2 = \frac{1}{N} \sum_{i'=1}^{N} \langle \sigma_{i'}^2 \rangle. \tag{5}$$

Instead, we have prefered to use the average of quadrupolar order parameteres of the layers given as

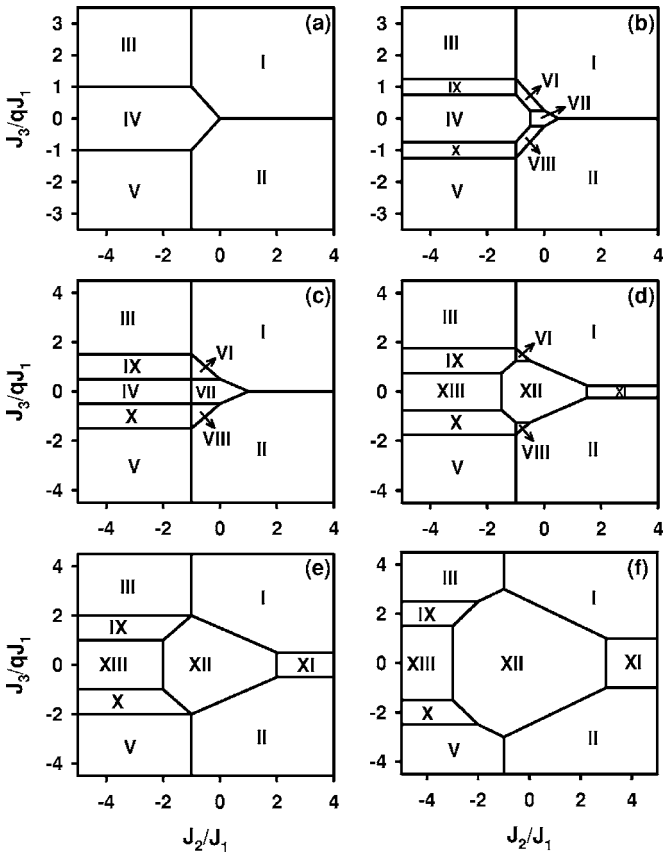

FIG. 2. The six distinct ground-state phase diagrams of the two-layer spin-1 Ising model with (a) $D/qJ_1 \geq 0$, (b) $D/qJ_1 = -0.25$, (c) $D/qJ_1 = -0.5$, (d) $D/qJ_1 = -0.75$, (e) $D/qJ_1 = -1.0$, and (f) $D/qJ_1 = -1.5$. Because of the competition between the crystal field and the bilinear interactions new configurations appear and as D/qJ_1 becomes more negative the paramagnetic configurations are preferred, see Table I.

$$Q = \frac{1}{2}(Q_1 + Q_2), \tag{6}$$

which is used to distinguish the P_+ and P_- phases of the paramagnetic phase corresponding to (i) $m=0$, $Q>2/3$ and (ii) $m=0$, $Q<2/3$, respectively.

Before obtaining the phase diagrams, first we have to study analytically the effects of the crystal field on the ground states, i.e., the phase diagrams of the model at zero absolute temperature. The ground-state energy in units of J_1 may be described by the following Hamiltonian:

$$\frac{E}{qJ_1} = -\sum_{\langle plaq \rangle} \left[\frac{J_1}{J_1} S_i S_j + \frac{J_2}{J_1} \sigma_{i'} \sigma_{j'} + \frac{J_3}{qJ_1} (S_i \sigma_{i'} + S_j \sigma_{j'}) + \frac{D}{qJ_1} (S_i^2 + S_j^2 + \sigma_{i'}^2 + \sigma_{j'}^2) \right], \tag{7}$$

where the summation goes over all plaquettes and each plaquette consists of four nearest-neighbor pair of the two-layer system with one pair, $\langle ij \rangle$, on G_1, one pair, $\langle i'j' \rangle$, on G_2, and two pairs, $\langle ii' \rangle$ and $\langle jj' \rangle$, connecting G_1 and G_2.

TABLE I. Ground-state configurations.

I	↑ ↑ ↑ ↑	VI	↑ ↑ ↑ ○	XI	○ ○ ↑ ↑
II	↑ ↑ ↓ ↓	VII	↑ ↑ ○ ○	XII	○ ○ ○ ○
III	↑ ↓ ↑ ↓	VIII	↑ ↑ ○ ↓	XIII	○ ○ ↑ ↓
IV	↑ ↑ ↑ ↓	IX	↑ ○ ↑ ↓		
V	↑ ↓ ↓ ↑	X	↑ ○ ↓ ↑		

The ground-state phase diagrams with respect to the crystal field change are obtained for $J_1>0$ on the $(J_2/J_1, J_3/qJ_1)$ plane for given values of D/qJ_1 and presented in Figs. 2(a)–2(f). This is done by comparing the values of the dimensionless energy E/qJ_1 for different spin configurations and then the ground-state configuration is the one with the lowest energy for given values of J_2/J_1, J_3/qJ_1, and D/qJ_1. As a result, we have obtained the thirteen different types of ground-state configurations shown in Table I.

As shown in Fig. 2, the different ground-state configurations appearing in Table I are separated by the multiphase lines. The connection points of these lines form the multiphase points where more than one ground-state configurations can coexist as in the multiphase lines. When $D/qJ_1 \geq 0.0$, the model only presents the first five configurations, ferromagnetic (F), compensated (C), mixed (M), antiferromagnetic (A), and surface ferromagnetic (SF) as explained in [43]. However, when D/qJ_1 becomes more and more negative owing to the competition between the bilinear interactions and D/qJ_1, the configurations are seen to appear which tries to take the system towards the paramagnetic configurations. For example, for $D/qJ_1=-0.25$ and -0.5, the additional configurations VI–X has appeared as shown in Figs. 2(b) and 2(c), respectively, but for $D/qJ_1<-0.5$ the configurations IV and VII of Figs. 2(b) and 2(c) is replaced with XIII and XII in Figs. 2(d)–2(f), besides the appearance of the new configuration XI. Therefore, it is now obvious that the crystal field effects does change the ground-state configurations of the model drastically. These different ground-state configurations give us valuable insight for obtaining phase diagram at higher temperatures.

III. THE ORDER PARAMETERS AND THE FREE ENERGY OF THE BILAYER SYSTEM

We are now ready to obtain the order-parameters and the free energy of the model in terms of the recursion relations on the bilayer Bethe lattice. Thus, first we have to obtain the partition function by using the Ising Hamiltonian given in Eq. (1). It is going to be assumed that adjacent NN spins of G_1 and G_2 are considered as pairs, so we employ the use of the pairwise approach [21]. The first pair deep inside the bilayer lattice is called the central pair which forms the first-generation spins. This central pair of spins connected by q NN spin pairs, i.e., coordination number, which forms the second generation spins. Each pair of spins in the second generation is joined to $(q-1)$ NN's. Therefore, in total the second generation has $q(q-1)$ NN's which form the third generation and so on to infinity. As a result each spin has $(q+1)$ NN spins, q from the layer it belongs to and one from the adjacent layer.

The partition function is defined as

$$Z = \sum_{All\ Config.} e^{-\beta\mathcal{H}} = \sum_{Spc} P(Spc), \tag{8}$$

and is to be obtained in terms of the recursion relations and, where $P(Spc)$ can be thought of as an unnormalized probability distribution. If the bilayer Bethe lattice is cut at the central site with pair of spins $(\sigma_{0'}, S_0)$ then it splits up into q identical branches. Each of these is a rooted tree at the central site. It should be mentioned that the phrase *spin site* refers to the sites of the spins while the word *site* refers to the sites of the pair of spins, such as central site, first site, etc…As a result, $P(\{\sigma_{0'}, S_0\})$ for the central pair may be written as

$$P(\{\sigma_{0'}, S_0\}) = \exp[\beta(J_3 S_0 \sigma_{0'} + D S_0^2 + D\sigma_{0'}^2)] \times \prod_{j=1}^{q} Q_n[(\sigma_{0'}, S_0)|(\sigma, S)^j], \tag{9}$$

where $(\sigma, S)^j$ indicates the pairs of the spins of the jth subtree other than the central pair $(\sigma_{0'}, S_0)$, the suffix n denotes the fact that the subtree has n shells, i.e., n steps from root to the boundary sites and

$$Q_n[(\sigma_{0'}, S_0)|(\sigma, S)^j] = \exp\Big[\beta\Big(J_1 S_0 S_1 + J_2 \sigma_{0'}\sigma_{1'} + J_3 \sigma_{1'} S_1 + D(S_1^2 + \sigma_{1'}^2) + J_1 \sum_{\langle ij \rangle} S_i S_j + J_2 \sum_{\langle i'j' \rangle} \sigma_{i'}\sigma_{j'} + J_3 \sum_{\langle ii' \rangle} S_i \sigma_{i'} + D\sum_i S_i^2 + D\sum_{i'} \sigma_{i'}^2\Big)\Big]. \tag{10}$$

The first three summations in the last equation are over all edges of the subtree other than the edge (0, 1) of the pairs in G_1, $(0', 1')$ of the pairs in G_2 and $(1, 1')$ of the pairs among the layers, respectively, and the summation over i and i' is over all spin sites other than the central spin sites. In addition, if the subtree with $n=1$ as shown in Fig. 1, for

instance the most-left subtree, is cut at the site 1 next to site 0, then it also decomposes into q pieces: one being the trunk with spin sites $(0,0')$ and $(1,1')$ and the rest being the identical branches. Each of these branches is a subtree like the original but with $(n-1)$ shells and $(q-1)$ NN pair of spins. Therefore,

$$Q_n[(\sigma_{0'},S_0)|(\sigma,S)^j] = \exp[\beta(J_1S_0S_1 + J_2\sigma_{0'}\sigma_{1'} + J_3S_1\sigma_{1'} + DS_1^2 + D\sigma_{1'}^2)] \times \prod_{k=1}^{q-1} Q_{n-1}[(\sigma_{1'},S_1)|(\sigma,S)^k], \quad (11)$$

where $(\sigma,S)^k$ denotes kth branch of the sub-subtree, i.e., $n=2$. Thus the formulation continues in this way by taking n steps from the central pair to the boundary sites, and in the thermodynamic limit $n\to\infty$, where the surface effects may be neglected. The function $g_n(\sigma_0',S_0)$ is the partition function of a separate branch and defined as

$$g_n(\sigma_{0'},S_0) = \sum_{\langle\sigma_{1'},S_1\rangle} \exp[\beta(J_1S_0S_1 + J_2\sigma_{0'}\sigma_{1'} + J_3S_1\sigma_{1'} + DS_1^2 + D\sigma_{1'}^2)] \times g_{n-1}^{q-1}(\sigma_{1'},S_1), \quad (12)$$

and may be obtained explicitly by summing over all the spin states, which yields nine different functions depending on the values of the central pair spins $\sigma_{0'}$ and S_0, each having the spin values ±1 and 0, in terms of the bilinear interactions and crystal field. As a result, we are now ready to introduce the eight recursion relations, $X^{(i)}$ with $(i=1,\ldots,8)$, as the ratios of the g_n functions as

$$X^1 = \frac{g_n(+,+)}{g_n(0,0)}, \quad X^2 = \frac{g_n(+,0)}{g_n(0,0)}, \quad X^3 = \frac{g_n(+,-)}{g_n(0,0)}, \quad X^4 = \frac{g_n(0,+)}{g_n(0,0)},$$
$$X^5 = \frac{g_n(0,-)}{g_n(0,0)}, \quad X^6 = \frac{g_n(-,+)}{g_n(0,0)}, \quad X^7 = \frac{g_n(-,0)}{g_n(0,0)}, \quad X^8 = \frac{g_n(-,-)}{g_n(0,0)}. \quad (13)$$

As explained above, we can easily obtain the recursion relations from Eqs. (12) and (13):

$$X_n^1 = f_1(X_{n-1}^1,X_{n-1}^2,X_{n-1}^3,X_{n-1}^4,X_{n-1}^5,X_{n-1}^6,X_{n-1}^7,X_{n-1}^8),$$
$$X_n^2 = f_2(X_{n-1}^1,X_{n-1}^2,X_{n-1}^3,X_{n-1}^4,X_{n-1}^5,X_{n-1}^6,X_{n-1}^7,X_{n-1}^8),$$
$$X_n^3 = f_3(X_{n-1}^1,X_{n-1}^2,X_{n-1}^3,X_{n-1}^4,X_{n-1}^5,X_{n-1}^6,X_{n-1}^7,X_{n-1}^8),$$
$$X_n^4 = f_4(X_{n-1}^1,X_{n-1}^2,X_{n-1}^3,X_{n-1}^4,X_{n-1}^5,X_{n-1}^6,X_{n-1}^7,X_{n-1}^8),$$
$$X_n^5 = f_5(X_{n-1}^1,X_{n-1}^2,X_{n-1}^3,X_{n-1}^4,X_{n-1}^5,X_{n-1}^6,X_{n-1}^7,X_{n-1}^8),$$
$$X_n^6 = f_6(X_{n-1}^1,X_{n-1}^2,X_{n-1}^3,X_{n-1}^4,X_{n-1}^5,X_{n-1}^6,X_{n-1}^7,X_{n-1}^8),$$
$$X_n^7 = f_7(X_{n-1}^1,X_{n-1}^2,X_{n-1}^3,X_{n-1}^4,X_{n-1}^5,X_{n-1}^6,X_{n-1}^7,X_{n-1}^8),$$
$$X_n^8 = f_8(X_{n-1}^1,X_{n-1}^2,X_{n-1}^3,X_{n-1}^4,X_{n-1}^5,X_{n-1}^6,X_{n-1}^7,X_{n-1}^8), \quad (14)$$

where the explicit definitions of $f_i(X_{n-1}^{(i)})$ with $(i=1,\ldots,8)$ functions are given in the Appendix .

Through $X_n^{(i)}$ with $(i=1,\ldots,8)$, one can express the dipolar and quadrupolar order parameters and other thermodynamic quantities, so we can say that in the thermodynamic limit $(n\to\infty)X^{(i)}$ with $(i=1,\ldots,8)$ determine the states of the system. For this reason the recursion relations can also be called the equations of state for the bilayer Ising model. The magnetizations of the first and the second layer are calculated as

$$m_1 = \langle S_0\rangle = [e^{\beta(J_3+2D)}(X_n^1)^q - e^{\beta(-J_3+2D)}(X_n^3)^q + e^{\beta D}(X_n^4)^q - e^{\beta D}(X_n^5)^q + e^{\beta(-J_3+2D)}(X_n^6)^q - e^{\beta(J_3+2D)}(X_n^8)^q]/D_2, \quad (15)$$

$$m_2 = \langle \sigma_0'\rangle = [e^{\beta(J_3+2D)}(X_n^1)^q + e^{\beta D}(X_n^2)^q + e^{\beta(-J_3+2D)}(X_n^3)^q - e^{\beta(-J_3+2D)}(X_n^6)^q - e^{\beta D}(X_n^7)^q - e^{\beta(J_3+2D)}(X_n^8)^q]/D_2, \quad (16)$$

and the spin-spin correlation function between the adjacent spins of the layers are expressed by

$$\rho = [e^{\beta(J_3+2D)}(X_n^1)^q - e^{\beta(-J_3+2D)}(X_n^3)^q - e^{\beta(-J_3+2D)}(X_n^6)^q + e^{\beta(J_3+2D)}(X_n^8)^q]/D_2 - m_1m_2, \quad (17)$$

and the quadrupolar moments of the layers are obtained,

$$Q_1 = \langle S_0^2\rangle = [e^{\beta(J_3+2D)}(X_n^1)^q + e^{\beta(-J_3+2D)}(X_n^3)^q + e^{\beta D}(X_n^4)^q + e^{\beta D}(X_n^5)^q + e^{\beta(-J_3+2D)}(X_n^6)^q + e^{\beta(J_3+2D)}(X_n^8)^q]/D_2, \quad (18)$$

$$Q_2 = \langle \sigma_0'^2\rangle = [e^{\beta(J_3+2D)}(X_n^1)^q + e^{\beta D}(X_n^2)^q + e^{\beta(-J_3+2D)}(X_n^3)^q + e^{\beta(-J_3+2D)}(X_n^6)^q + e^{\beta D}(X_n^7)^q + e^{\beta(J_3+2D)}(X_n^8)^q]/D_2, \quad (19)$$

where

$$D_2 = e^{\beta(J_3+2D)}(X_n^1)^q + e^{\beta D}(X_n^2)^q + e^{\beta(-J_3+2D)}(X_n^3)^q + e^{\beta D}(X_n^4)^q + e^{\beta D}(X_n^5)^q + e^{\beta(-J_3+2D)}(X_n^6)^q + e^{\beta D}(X_n^7)^q + e^{\beta(J_3+2D)}(X_n^8)^q + 1. \quad (20)$$

In addition to the thermal behaviors of the order parameters, we also need the free energy in terms of the recursion relations to obtain the phase diagram of the model. Therefore, the free energy of the bilayer Bethe lattice is calculated as

$$-\beta F = \ln(D_2) + \frac{q}{2-q}\ln(D_1), \quad (21)$$

where D_2 and D_1 are given in Eq. (20) and in the Appendix, respectively. In order to determine the first-order

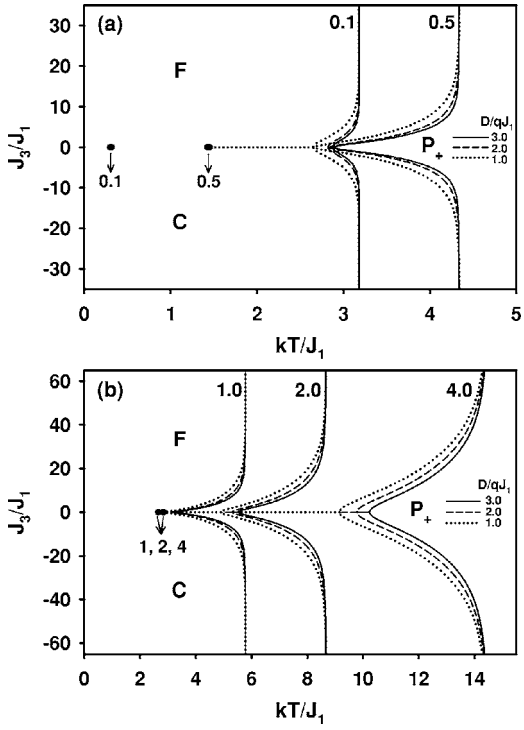

FIG. 3. The model gives only the first-order phase transition lines until (•) along the $J_3/J_1=0$ axis and the second-order lines as shown with dotted, dashed, and solid lines corresponding $D/qJ_1=1,2$, and 3, respectively, and obtained for (a) $J_2/J_1=0.1$ and 0.5 and (b) $J_2/J_1=1$, 2, and 4.

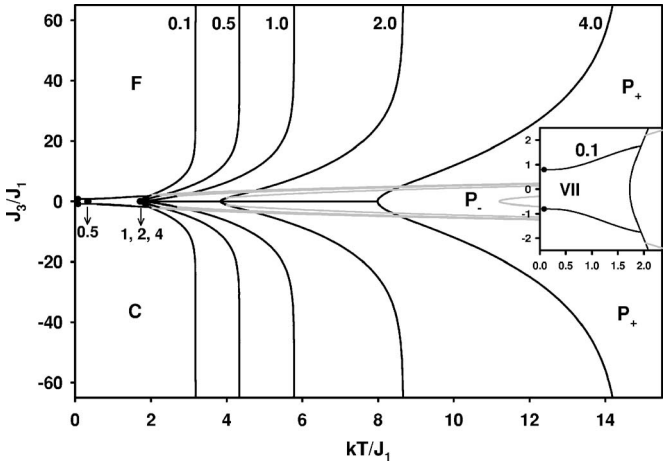

FIG. 4. For $D/qJ_1=-0.25$ additional first-order lines and tricritical points appear for $J_2/J_1=0.1$ as shown in the inset. The behaviors of the other lines for $J_2/J_1=0.5$, 1, 2, and 4 are the same as in Fig. 3. The gray lines indicate the boundary between the P_+ and P_- phases.

phase transition temperatures one has to use a free-energy analysis. It is worthwhile to mention that in solving the recursion relations, one has to assign initial values for each of them. Therefore, varying the initial values may result in different solutions for all the thermodynamic functions including the free energy. Thus, the temperature at which these free energy solutions combine is the first-order phase transition temperature.

In concluding this section, we should remark that in order to obtain the thermal behaviors of the order parameters and the free energy, first the recursion relations are calculated by using an iteration scheme, then the found values of the recursion relations are inserted into the definitions of the order parameters and the free energy which are the functions of the bilinear interactions, crystal field, and coordination number q, which is fixed at 4.

IV. THE CRYSTAL FIELD EFFECT ON THE PHASE DIAGRAMS OF THE BILAYER BETHE LATTICE

After having obtained the necessary equations for the calculation of the order parameters, i.e., the total and staggered magnetizations, the average of quadrupolar moment and the spin-spin correlation function, and the free energy of the bilayer Bethe lattice in the existence of the crystal field, we are now ready to obtain the phase diagrams on the $(J_3/J_1, kT/J_1)$ plane. It is a standard definition that the phase transition is the second-order type when the total or staggered magnetizations change continuously from one phase to the other and is the first-order type if these magnetizations give a discontinuity during the phase transition. As a result, the phase diagrams are constructed by considering the thermal change of the order parameters and the free energy and, the ground-state phase diagram of the model for the coordination number $q=4$. We have obtained phase diagrams depending on the values of the crystal field and J_2/J_1 by using the six different characteristical ground-state phase diagrams of the model.

The first phase diagrams of the model are obtained for the positive values of D/qJ_1 for $J_2/J_1=0.1$ and 0.5, see Fig. 3(a), and $J_2/J_1=1$, 2 and 4 as shown in Fig. 3(b). The solid, dashed, and dotted lines are used to label the second-order phase transition lines for $D/qJ_1=3$, 2, and 1, respectively, and the tricritical points are labeled with the values of J_2/J_1. One can divide these phase diagrams into three sections; that is the left- and right-hand sides of the tricritical point shown with a solid circle (•) divides the two ordered phases, i.e., ferromagnetic (F) and compensated (C), with the first- and second-order phase transition lines at $J_3/J_1=0$, respectively, and from the end of this second-order line two more branches of the second-order lines emerge symmetrically, where the upper and the lower parts of these lines separate the phases (F) and (C) from the P_+ phase, as shown in Fig. 3. It should be mentioned that the tricritical points for $J_2/J_1=1$, 2, and 4 almost seem to be at the same temperature, but as J_2/J_1 decreases, for example, 0.1 and 0.5 in Fig. 3(a), the tricritical points are seen at lower and different temperatures, see also Refs. [21,43]. One last point of this figure is that the interlayer interaction aligns the spins of the layers in the same direction when positive and oppositely when negative, since the crystal field acts on the squares of the spins, thus, the symmetry of the model with respect J_3/J_1 axes will not be spoiled by the crystal field effects. The decrease in D/qJ_1 makes the configurations move towards wider paramagnetic regions, which is also obvious from the ground-state phase diagrams. In addition, as J_3/J_1 increases, the crystal field cannot overcome the ordering effect of J_3/J_1

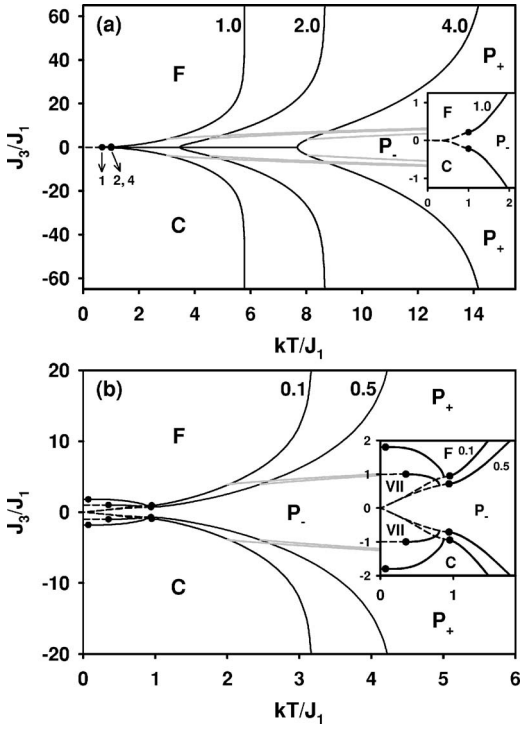

FIG. 5. $D/qJ_1=-0.5$. (a) For $J_2/J_1=2$ and 4, the critical lines behave as before but $J_2/J_1=1$, the first-order line along $J_3/J_1=0$ axis, is separated into two branches and (b) $J_2/J_1=0.1$ and 0.5, the configuration VII is also seen.

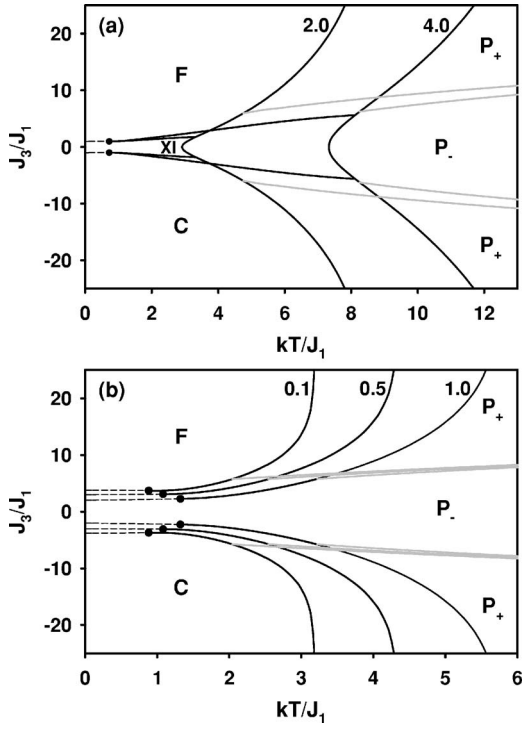

FIG. 6. $D/qJ_1=-0.75$. (a) For $J_2/J_1=2$ and 4, the configuration XI is also seen. (b) $J_2/J_1=0.1$, 0.5, and 1, now the P_- phase is also available at zero temperature.

anymore, thus at higher J_3/J_1 these second-order lines for the values of D/qJ_1 overlap.

The next phase diagram is calculated for $D/qJ_1=-0.25$ and illustrated in Fig. 4. According to the ground-state phase diagram for positive J_2/J_1 until 0.5 a new configuration, i.e., configuration VII as given in Table I, appears in comparison with the previous figure. The behaviors of the second-order lines for $J_2/J_1=0.5$, 1, 2, and 4 has not changed but when $J_2/J_1=0.1$ two first-order lines appear at $J_3/J_1=\pm 0.8$ which continue until the corresponding (•) from which the second-order lines emerge. The lower and upper parts of these lines separate the compensated and the ferromagnetic phases from the phase VII, respectively, which end on the other second-order line which is the same as in Fig. 3. Because of the crystal field effect, the first-order lines now also seen for $J_3/J_1 \neq 0.0$.

For $D/qJ_1=-0.5$, the second-order lines for $J_2/J_1=2$ and 4 of Fig. 5(a) are the same as before, when it equals to 1.0 two (•)'s appear which correspond to the multiphase point of Fig. 2(c). Then the two first-order lines symmetrically and asymptotically go to $J_3/J_1=0.0$ where they combine and continue until the zero temperature. In Fig. 5(b) for $J_2/J_1=0.1$ and 0.5, the critical lines not only show the similar behaviors as in the case with $J_2/J_1=1.0$, but now also some other critical lines appear. These critical lines for each J_2/J_1 seen to be as two first-order lines starting from the zero temperature symmetrically with respect to J_3/J_1 axes. At the ends of them two more (•)'s appear and from them two second-order lines emerge and continue until combining to their corresponding first-order lines, called the critical end point, for each J_2/J_1.

In the next figures for $D/qJ_1=-0.75$, again the behaviors of the critical lines are the same as with the inset of Fig. 4 but having the configuration XI as given in Fig. 2(d) and

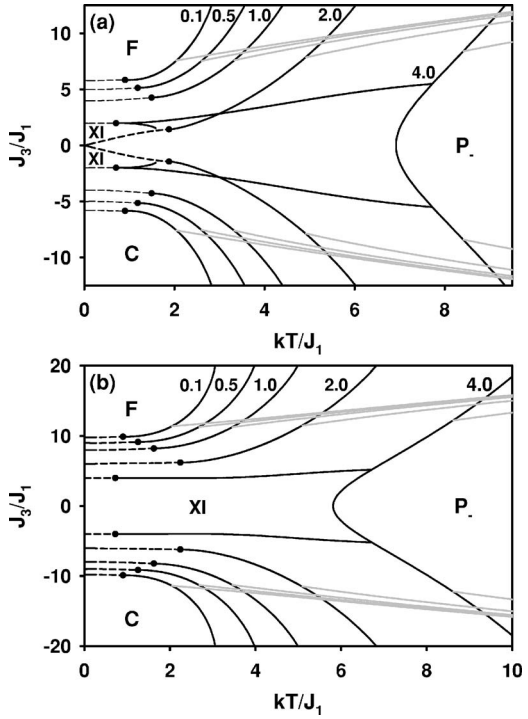

FIG. 7. (a) $D/qJ_1=-1.0$ and (b) $D/qJ_1=-1.5$. It is obvious that as the crystal field become more negative the boundaries of the configurations XI and XII, or the P_- phase, increase.

illustrated in Fig. 6(a). In Fig. 6(b), two first-order lines for each of $J_2/J_1=0.1$, 0.5, and 1.0 emerge symmetrically, which are seen at higher values of J_3/J_1 as J_2/J_1 becomes smaller; this is also obvious from the slopes of the multiphase lines separating the phase XII (P_- phase) from the phases I and II of Fig. 2(d). Again from the ends of these lines at the (•)'s the corresponding second-order lines come out. It is now very clear that the crystal field effects are dominant to the interlayer interactions, thus, even at zero temperature the P_- phase appears.

Finally, the last phase diagrams are given in Figs. 7(a) and 7(b) and obtained for $D/qJ_1=-1.0$ and -1.5. When comparing the ground-state phase diagrams in Figs. 2(d)–2(f), they all have the same configurations but with different shapes in the antiferromagnetic region, however, in the ferromagnetic region the only differences are the growing of the phases XI and XII. Therefore, the obtained phase diagrams of the corresponding $D/qJ_1=-1.0$ and -1.5 are similar with the previous phase diagrams of this work.

Meanwhile, we have also separated the paramagnetic phase into the phases P_+ and P_- by studying the thermal variations of the quadrupolar moments of the layers. The boundary between these two phases corresponding to $Q=2/3$ is indicated with gray solid lines in the phase diagrams. Two boundary lines symmetrically emerge from the second-order phase transition lines for $J_3/J_1>0$ and $J_3/J_1<0$, i.e, the second-order lines separating the (F) and (C) phases from the paramagnetic phases, respectively, except in Fig. 4 for $J_2/J_1=4$, this line does not combine with the second-order line but instead makes a half-closed loop at higher temperatures. The region between these two lines corresponds to the P_- phase, while the exterior regions correspond to the P_+ phase. It is well-known that the quadrupolar order-parameter depends strongly on the values of the crystal field. We have found that for positive values of the crystal field the system only presents the P_+ phase as in Fig. 3, but for the negative values the P_- phase also appears as in the rest of the figures.

In concluding this section we should note that by using the order-parameters, free energy and the ground state phase diagrams of the model, we have constructed the phase diagrams on the $(kT/J_1, J_3/J_1)$ plane showing the crystal field effect on the system in a great detail.

V. CONCLUSIONS

As an extension of bilayer spin-1 Ising model [43], we have studied the same model with the inclusion of the crystal field to see its effects on the phase diagrams with $q=4$. It is found that for the positive values of D/qJ_1 the phase diagrams does not change too much except for the extension of the paramagnetic phases towards the zero temperature. But as D/qJ_1 becomes more and more negative the phase diagrams change drastically, this is caused by the competition with the interlayer bilinear interaction. This is also obvious from the ground-state phase diagrams, since at higher negative values the zeros of the configurations, i.e., paramagnetic phase regions, increase. We should also note that for the positive values of D/qJ_1 the phase diagrams of the bilayer spin-1/2 [21] and spin-1 [43] are similar, except for the negative values, the changes are now clear to see.

The results of this work is only obtained for the ferromagnetic coupling in each layer and ferro- or antiferromagnetic couplings between the layers. While the studies of the antiferromagnetic coupling of each layer to examine the crystal field effects on the phase diagrams and also increasing the number of layers may have been much more interesting, we have to say that the obtaining of the phase diagrams in this study was quite overwhelming.

APPENDIX

The explicit definitions of $f_i(X_{n-1}^{(i)})$ $(i=1,\ldots,8)$ functions are given as

$$f_1(X_n^{(i)}) = [e^{\beta(J_1+J_2+J_3+2D)}(X_n^1)^{q-1} + e^{\beta(J_2+D)}(X_n^2)^{q-1} + e^{\beta(-J_1+J_2-J_3+2D)}(X_n^3)^{q-1} + e^{\beta(J_1+D)}(X_n^4)^{q-1} + e^{\beta(-J_1+D)} \times (X_n^5)^{q-1} + e^{\beta(J_1-J_2-J_3+2D)}(X_n^6)^{q-1} + e^{\beta(-J_2+D)}(X_n^7)^{q-1} + e^{\beta(-J_1-J_2+J_3+2D)}(X_n^8)^{q-1} + 1]/D_1,$$

$$f_2(X_n^{(i)}) = [e^{\beta(J_2+J_3+2D)}(X_n^1)^{q-1} + e^{\beta(J_2+D)}(X_n^2)^{q-1} + e^{\beta(J_2-J_3+2D)} \times (X_n^3)^{q-1} + e^{\beta D}(X_n^4)^{q-1} + e^{\beta D}(X_n^5)^{q-1} + e^{\beta(-J_2-J_3+2D)} \times (X_n^6)^{q-1} + e^{\beta(-J_2+D)}(X_n^7)^{q-1} + e^{\beta(-J_2+J_3+2D)}(X_n^8)^{q-1} + 1]/D_1,$$

$$f_3(X_n^{(i)}) = [e^{\beta(-J_1+J_2+J_3+2D)}(X_n^1)^{q-1} + e^{\beta(J_2+D)}(X_n^2)^{q-1} + e^{\beta(J_1+J_2-J_3+2D)}(X_n^3)^{q-1} + e^{\beta(-J_1+D)}(X_n^4)^{q-1} + e^{\beta(J_1+D)} \times (X_n^5)^{q-1} + e^{\beta(-J_1-J_2-J_3+2D)}(X_n^6)^{q-1} + e^{\beta(-J_2+D)}(X_n^7)^{q-1} + e^{\beta(J_1-J_2+J_3+2D)}(X_n^8)^{q-1} + 1]/D_1,$$

$$f_4(X_n^{(i)}) = [e^{\beta(J_1+J_3+2D)}(X_n^1)^{q-1} + e^{\beta D}(X_n^2)^{q-1} + e^{\beta(-J_1-J_3+2D)} \times (X_n^3)^{q-1} + e^{\beta(J_1+D)}(X_n^4)^{q-1} + e^{\beta(-J_1+D)}(X_n^5)^{q-1} + e^{\beta(J_1-J_3+2D)}(X_n^6)^{q-1} + e^{\beta D}(X_n^7)^{q-1} + e^{\beta(-J_1+J_3+2D)} \times (X_n^8)^{q-1} + 1]/D_1,$$

$$f_5(X_n^{(i)}) = [e^{\beta(-J_1+J_3+2D)}(X_n^1)^{q-1} + e^{\beta D}(X_n^2)^{q-1} + e^{\beta(J_1-J_3+2D)} \times (X_n^3)^{q-1} + e^{\beta(-J_1+D)}(X_n^4)^{q-1} + e^{\beta(J_1+D)}(X_n^5)^{q-1} + e^{\beta(-J_1-J_3+2D)}(X_n^6)^{q-1} + e^{\beta D}(X_n^7)^{q-1} + e^{\beta(J_1+J_3+2D)} \times (X_n^8)^{q-1} + 1]/D_1,$$

$$f_6(X_n^{(i)}) = [e^{\beta(J_1-J_2+J_3+2D)}(X_n^1)^{q-1} + e^{\beta(-J_2+D)}(X_n^2)^{q-1} + e^{\beta(-J_1-J_2-J_3+2D)}(X_n^3)^{q-1} + e^{\beta(J_1+D)}(X_n^4)^{q-1} + e^{\beta(-J_1+D)} \times (X_n^5)^{q-1} + e^{\beta(J_1+J_2-J_3+2D)}(X_n^6)^{q-1} + e^{\beta(J_2+D)}(X_n^7)^{q-1} + e^{\beta(-J_1+J_2+J_3+2D)}(X_n^8)^{q-1} + 1]/D_1,$$

$$f_7(X_n^{(i)}) = [e^{\beta(-J_2+J_3+2D)}(X_n^1)^{q-1} + e^{\beta(-J_2+D)}(X_n^2)^{q-1} + e^{\beta(-J_2-J_3+2D)}(X_n^3)^{q-1} + e^{\beta D}(X_n^4)^{q-1} + e^{\beta D}(X_n^5)^{q-1} + e^{\beta(J_2-J_3+2D)}(X_n^6)^{q-1} + e^{\beta(J_2+D)}(X_n^7)^{q-1} + e^{\beta(J_2+J_3+2D)} \times (X_n^8)^{q-1} + 1]/D_1,$$

with

$$f_8(X_n^{(i)}) = [e^{\beta(-J_1-J_2+J_3+2D)}(X_n^1)^{q-1} + e^{\beta(-J_2+D)}(X_n^2)^{q-1} + e^{\beta(J_1-J_2-J_3+2D)}(X_n^3)^{q-1} + e^{\beta(-J_1+D)}(X_n^4)^{q-1} + e^{\beta(J_1+D)} \times (X_n^5)^{q-1} + e^{\beta(-J_1+J_2-J_3+2D)}(X_n^6)^{q-1} + e^{\beta(J_2+D)}(X_n^7)^{q-1} + e^{\beta(J_1+J_2+J_3+2D)}(X_n^8)^{q-1} + 1]/D_1,$$

$$D_1 = e^{\beta(J_3+2D)}(X_n^1)^{q-1} + e^{\beta D}(X_n^2)^{q-1} + e^{\beta(-J_3+2D)}(X_n^3)^{q-1} + e^{\beta D}(X_n^4)^{q-1} + e^{\beta D}(X_n^5)^{q-1} + e^{\beta(-J_3+2D)}(X_n^6)^{q-1} + e^{\beta D}(X_n^7)^{q-1} + e^{\beta(J_3+2D)}(X_n^8)^{q-1} + 1.$$

[1] Digest of the 13th International Colloq. on Magnetic Films and Surfaces, Glasgow, 1991 (unpublished).

[2] M. N. Baibich, J. M. Broto, A. Fert, F. Nguyen Van Dau, and F. Petroff, P. Etienne, G. Creuzet, A. Friederich, and J. Chazelas, Phys. Rev. Lett. **61**, 2472 (1988); G. Binasch, P. Grunberg, F. Saurenbach, and W. Zinn, Phys. Rev. B **39**, 4828 (1989).

[3] J. Sayama, T. Asahi, K. Mizutani, and T. Osaka, J. Phys. D **37**, L1 (2004).

[4] R. Wu and A. J. Freeman, Phys. Rev. B **45**, 7205 (1992); M. Donath, J. Phys.: Condens. Matter **11**, 9421 (1999).

[5] S. W. Sun and R. C. O'Handley, Phys. Rev. Lett. **66**, 2798 (1991); G. Bochi, O. Song, and R. C. O'Handley, Phys. Rev. B **50**, 2043 (1994).

[6] L. Bahmad, A. Benyoussef, and H. Ez-Zahraouy, Surf. Sci. **536**, 114 (2003); P. J. Jensen and H. Dreysse, Phys. Rev. B **66**, 220407(R) (2002); A. Lipowski and M. Suzuki, Physica A **198**, 227 (2000); M. Bengrine, A. Benyoussef, H. Ez-Zahraouy, and F. Mhirech, Physica A **268**, 149 (1999); L. Bahmad, A. Benyoussef, and H. Ez-Zahraouy, J. Magn. Magn. Mater. **238**, 115 (2002).

[7] T. Kaneyoshi and S. Shin, Physica A **284**, 195 (2000); Y. M. Seidov and G. R. Shaulov, J. Phys.: Condens. Matter **6**, 9621 (1994); L. Peliti and M. Saber, Physica A **262**, 505 (1999); B. Laaboudi, M. Saber, and M. Kerouad, Phys. Status Solidi B **212**, 153 (1999); T. Bouziane, *ibid.* **217**, 951 (2000); T. Bouziane and A. Belaaraj, *ibid.* **214**, 387 (1999); F. Dujardin, B. Stebe, A. Ainane, and M. Saber, Chin. J. Phys. (Taipei) **37**, 479 (1999); L. Bahmad, A. Benyoussef, A. El Kenz, and H. Ez-Zahraouy, M. J.Condensed Matter **3**, 23 (2000).

[8] A. M. Ferrenberg and D. P. Landau, J. Appl. Phys. **70**, 6215 (1991); D. P. Landau and K. Binder, Phys. Rev. B **41**, 4786 (1990); P. Henelius, P. Frobrich, P. J. Kuntz, C. Timm, and P. J. Jensen, Phys. Rev. B **66**, 094407 (2002); H. Ez-Zahraouy, L. Bahmad, and A. Benyoussef, Physica A **358**, 86 (2005); S. H. Tsai, D. P. Landau, and T. C. Schulthess, J. Appl. Phys. **91**, 6884 (2002); H. Liu, J. Ni, and B. Gu, Eur. Phys. J. B **26**, 261 (2002).

[9] K. Hida, J. Phys. Soc. Jpn. **65**, 594 (1996).

[10] Z. B. Li, Z. Shuai, Q. Wang, H. J. Luo, and L. Schülke, J. Phys. A **34**, 606 (2001).

[11] J. Oitmaa and I. G. Enting, J. Phys. A **8**, 1097 (1975).

[12] J. Wosiek, Phys. Rev. B **49**, 15023 (1994).

[13] P. J. Jensen and K. H. Bennemann, Phys. Rev. B **42**, 849 (1990).

[14] Y. Zhou, J. Chen, Z. Rong, and D. L. Lin, Phys. Lett. A **298**, 287 (2002).

[15] Zheng Weihong, Phys. Rev. B **59**, 387 (1999).

[16] G. Wiatrowski, G. Bayreuther, and K. Pruegl, J. Magn. Magn. Mater. **196-197**, 26 (1999).

[17] A. Khater, M. A. Ghantous, and M. Fresnau, J. Phys. D **35**, 951 (2002).

[18] J. L. Monroe, Physica A **335**, 563 (2004).

[19] J. L. Monroe, Phys. Rev. E **71**, 017105 (2005).

[20] M. L. Lyra and C. R. da Silva, Phys. Rev. B **47**, 526 (1993).

[21] C.-K. Hu, N. Sh. Izmailian, and K. B. Oganesyan, Phys. Rev. E **59**, 6489 (1999).

[22] M. Blume, V. J. Emery, and R. B. Griffiths, Phys. Rev. A **4**, 1071 (1971).

[23] J. Lajzerowicz and J. Sivardière, Phys. Rev. A **11**, 2079 (1975); J. Sivardière and J. Lajzerowicz, *ibid.* **11**, 2090 (1975); , **11**, 2101 (1975).

[24] M. Schick and W. -H. Shih, Phys. Rev. B **34**, 1797 (1986).

[25] K. E. Newman and J. D. Dow, Phys. Rev. B **27**, 7495 (1983).

[26] D. Mukamel and M. Blume, Phys. Rev. A **10**, 610 (1974).

[27] S. A. Kivelson, V. J. Emery, and H. Q. Lin, Phys. Rev. B **42**, 6523 (1990).

[28] E. Vives, T. Castan, and P. A. Lindgard, Phys. Rev. B **53**, 8915 (1996).

[29] A. N. Berker and M. Wortis, Phys. Rev. B **14**, 4946 (1976).

[30] E. F. Sarmento and T. Kaneyoshi, Phys. Rev. B **40**, 2529 (1989).

[31] H. S. Youn and G. B. Hess, Phys. Rev. Lett. **64**, 918 (1990); H. S. Youn, X. F. Meng, and G. B. Hess, Phys. Rev. B **48**, 14556 (1993).

[32] P. B. Weichman, P. Day, and D. Goodstein, Phys. Rev. Lett. **74**, 418 (1995).

[33] P. J. Jensen and K. H. Bennemann, Phys. Rev. B **52**, 16012 (1995).

[34] J. W. Tucker, T. Balcerzak, M. Gzik, and A. Sukiennicki, J. Magn. Magn. Mater. **187**, 381 (1998).

[35] P. J. Jensen, K. H. Bennemann, P. Poulpoulos, M. Farle, F. Wilhelm, and K. Baberschke, Phys. Rev. B **60**, R14994 (1999); P. J. Jensen, K. H. Bennemann, K. Baberschke, P. Poulpoulos, and M. Farle, J. Appl. Phys. **87**, 6692 (2000).

[36] L. Bahmad, A. Benyoussef, and H. Ez-Zahraouy, Surf. Sci. **552**, 1 (2004); J. Magn. Magn. Mater. **251**, 115 (2002).

[37] A. Benyoussef, H. Ez-Zahraouy, H. Mahboub, and M. J. Ouaz-

zani, Physica A **326**, 220 (2003).
[38] A. Saber, A. Ainane, F. Dujardin, N. El Aouad, M. Saber, and B. Stébé, J. Phys.: Condens. Matter **12**, 43 (2000); A. Saber, A. Ainane, F. Dujardin, N. El Aouad, M. Saber, and B. Stébé, J. Phys.: Condens. Matter **11**, 2087 (1999).
[39] M. Kurota, R. Kikuchi, and T. Watari, J. Chem. Phys. **21**, 434 (1953); C. Domb, Adv. Phys. **9**, 208 (1960).
[40] C.-K. Hu and N. Sh. Izmailian, Phys. Rev. E **58**, 1644 (1998); N. Sh. Izmailian and C.-K. Hu, Physica A **254**, 198 (1998).
[41] J. W. Tucker, J. Magn. Magn. Mater. **195**, 733 (1999); E. Albayrak and M. Keskin, *ibid.* **261**, 196 (2003); E. Albayrak and A. Yigit, Physica A **349**, 471 (2005); E. Albayrak and A. Yigit, Phys. Status Solidi B **242**, 1510 (2005).
[42] R. J. Baxter, *Exactly Solved Models in Statistical Mechanics* (Academic Press, New York, 1982); N. Sh. Ananikian, A. R. Avakian, and N. Sh. Izmailian, Physica A **172**, 391 (1991); E. Albayrak and M. Keskin, J. Magn. Magn. Mater. **241**, 249 (2002).
[43] E. Albayrak and O. Canko, Physica A **373**, 363 (2007)